JOURNAL OF SPACECRAFT AND ROCKETS
Vol. 41, No. 4, July–August 2004

Numerical Simulation of Magnetohydrodynamic Flows

Jean-François Dietiker* and Klaus A. Hoffmann†
Wichita State University, Wichita, Kansas 67260-0044

The development of a versatile computational tool for the solution of turbulent magnetohydrodynamic flows is presented. The flow solver can simulate the full magnetohydrodynamic equations or simplified equations based on the low magnetic Reynolds number approximation. Both laminar and turbulent flows are investigated. The Baldwin–Lomax turbulence model evaluates the eddy viscosity to represent turbulence. Modifications accounting for the presence of a magnetic field are presented to extend its range of application to magnetohydrodynamic flows. The modification of the turbulence model is performed based on the turbulent Hartmann flow. The numerical solutions are compared with existing analytical solutions and experimental data, for low- and high-speed magnetohydrodynamic flows.

Nomenclature

A = coefficient of damping term in modified Baldwin–Lomax model
B = magnitude of the magnetic induction field
$\boldsymbol{B}$ = magnetic induction field, $\begin{bmatrix} B_x \\ B_y \\ B_z \end{bmatrix}$
$\bar{B}_x$, $\bar{B}_y$ = transformed components of the magnetic field in the computational space
c_p = specific heat at constant pressure, N · m/kg · K
$\boldsymbol{E}$ = flux vector in x direction (physical space)
$\boldsymbol{E}_c$ = electric field vector, $\begin{bmatrix} E_x \\ E_y \\ E_z \end{bmatrix}$
$\boldsymbol{E}_v$ = viscous flux vector in x direction (physical space)
$\bar{\boldsymbol{E}}$ = flux vector in ξ direction (computational space)
$\overline{\boldsymbol{E}_v}$ = viscous flux vector in ξ direction (computational space)
e_t = total energy
$\boldsymbol{F}$ = flux vector in y direction (physical space)
$\boldsymbol{F}_v$ = viscous flux vector in y direction (physical space)
$\bar{\boldsymbol{F}}$ = flux vector in η direction (computational space)
$\overline{\boldsymbol{F}_v}$ = viscous flux vector in η direction (computational space)
$\boldsymbol{H}$ = source term in physical space
Ha = Hartmann number
$\boldsymbol{H}_M$ = intermediate magnetic vector
$\bar{\boldsymbol{H}}$ = source term in computational space
J = Jacobian of transformation
k = thermal conductivity, turbulent kinetic energy, W/m · K
L = characteristic length, m
l = characteristic turbulent length scale, mixing length, m
M_∞ = freestream Mach number
Pr = Prandtl number
p = pressure
$\boldsymbol{Q}$ = unknown field vector
$\boldsymbol{Q}_h$ = heat flux vector, $\begin{bmatrix} q_x \\ q_y \\ q_z \end{bmatrix}$
$\bar{\boldsymbol{Q}}$ = unknown field vector in computational space
Re = Reynolds number
Re_m = magnetic Reynolds number
S = interaction parameter
$\boldsymbol{S}_{\mathrm{MHD}}$ = magnetohydrodynamics (MHD) source term in physical space
$\bar{\boldsymbol{S}}_{\mathrm{MHD}}$ = MHD source term in computational space
T = temperature
t = time
$\boldsymbol{U}$ = velocity vector, $\begin{bmatrix} u \\ v \\ w \end{bmatrix}$
V_t = characteristic turbulent velocity
x, y = space coordinate
y^+ = nondimensional distance to the wall
γ = ratio of specific heats
γ_2, γ_3 = damping function in the modified Baldwin–Lomax model
δ_{ij} = Kronecker delta
η_x, η_y = metrics of transformation
κ = von Kármán constant
λ = damping coefficients for the modified Baldwin–Lomax model
μ = dynamic viscosity, N · s/m^2
μ_{e0} = free space magnetic permeability, s/mho · m
μ_{t_i} = inner layer turbulent viscosity
μ_{t_o} = outer layer turbulent viscosity
ξ, η = generalized coordinates (computational space)
ξ_x, ξ_y = metrics of transformation
ρ = density
σ_e = electrical conductivity, mho/m
$\bar{\bar{\tau}}$ = stress tensor
ω = vorticity

Subscripts

w = property evaluated at the wall
∞ = freestream condition

Received 4 February 2003; revision received 15 July 2003; accepted for publication 17 July 2003.

*Visiting Assistant Professor, Department of Aerospace Engineering, 1845 Fairmount.
†Professor, Department of Aerospace Engineering, 1845 Fairmount. Associate Fellow AIAA.

Superscripts

$'$ = perturbation quantity
$*$ = nondimensional quantity
$-$ = Reynolds averaged quantity, quantity expressed in computational space

Introduction

MAGNETOHYDRODYNAMICS (MHD) is a branch of fluid dynamics that studies the interaction of an electrically conducting fluid with an electromagnetic field. The MHD effect has been investigated for engineering applications, for example, propulsion systems or power generators. MHD shows great potential in aerospace engineering because it offers the possibility of controlling the flow around a vehicle or even extracting energy from its surroundings.

When an electrically conducting fluid moves through a magnetic field, it produces an electric field and subsequently an electric current. The interaction of the induced electric current with the magnetic field creates a body force, called the Lorentz force, which acts on the fluid itself. MHD is mathematically represented by the combination of Maxwell's equations, governing the electromagnetic field, and Navier–Stokes equations governing the flowfield. The corresponding set of equations is known as the MHD equations. These equations must be solved to analyze MHD flows. There have been numerous attempts in solving these equations, starting from analytical or empirical methods. Because the governing equations are nonlinear partial differential equations, they can be analytically solved only for simple flows with restrictive assumptions on the flow or the magnetic field. Rossow[1] developed an approximate solution for an incompressible laminar flow over a flat plate subject to a uniform magnetic field. He showed that, as the magnetic field is increased, the skin friction and heat transfer are reduced. Other investigators have shown the same trend for other types of flows. Lykoudis developed a similarity solution for boundary-layer flows over a wedge.[2] The hypersonic MHD Couette flow was analytically solved by Bleviss.[3] This was an important step in the understanding of boundary-layer flows in the presence of magnetic fields. He also found that, for high Mach numbers, the presence of a magnetic field decreases the skin friction but increases the heat transfer. For hypersonic flows around blunt bodies, Bush[4] has shown that the shock standoff distance would increase and the surface pressure would decrease in the presence of a magnetic field. Lykoudis[5] developed an analytical solution for the shock standoff distance for hypersonic flows of an electrically conducting fluid around a sphere and a cylinder.

With the expansion of computational fluid dynamics, it has become possible to investigate MHD flows under less limiting conditions on the magnetic field or the flow properties. Palmer[6] numerically solved the flow past an axisymmetric blunt body. He computed the flowfield for both self-generated and applied magnetic field. He also considered the flow in thermal equilibrium and chemical nonequilibrium. The same increase in the standoff distance was obtained as for the existing analytical solutions. Because the MHD equations are hyperbolic in nature, numerical schemes based on characteristic formulation have been widely used. High-order Godunov schemes have been used for one-dimensional cases and shock tube problems (see Refs. 7–12). Riemann solvers associated with Godunov schemes have been proven to be robust and able to capture accurately the shock waves. More recently, modified Runge–Kutta schemes augmented with total variation diminishing (TVD) schemes have been used for one-dimensional and two-dimensional problems (see Refs. 13–17). The use of the TVD scheme as a postprocess stage allows good shock wave capturing with little or no spurious oscillation. This method requires the determination of the eigenvalues and eigenvectors of the system of equations. For the ideal one-dimensional case, the flow is described by a seven-wave system, whereas for the ideal two-dimensional case, an eight-wave system is obtained. It has been shown that the determination of the eigenvalues and eigenvectors of the system requires a mathematical modification of the governing equations due to a singularity in the Jacobian matrices (see Ref. 18). Recently, this scheme has been extended to the case where molecular viscosity and magnetic diffusivity are taken into consideration.[19]

Most supersonic and hypersonic flows are turbulent. Therefore, inclusion of turbulence in the computation of such flowfields is essential. It has been shown that the presence of a magnetic field could decrease the drag and heat transfer for laminar flows. It is, thus, important to investigate turbulent supersonic flowfields subject to magnetic fields to identify the overall effect of this combination.

Most of the research combining the effect of turbulence with MHD has been conducted for flows of liquid metals in simple geometries or in astrophysical applications, where the length scales are very large. Basic observations tend to show that the presence of a magnetic field would inhibit turbulence. Ferraro and Plumton[20] discussed the inhibition of turbulence by a magnetic field and suggested a criterion on the magnitude of the magnetic field that would tend to inhibit the onset of turbulence. Lykoudis[21] showed that for large values of the Hartmann number, the magnetic field (which enters the solution through the Hartmann number) has the same effect on the laminar layer as suction. His result was based on the laminar velocity profile in the case of a channel flow.

For simple engineering applications, the effect of the magnetic field on turbulence has been integrated into existing turbulence concepts or even turbulence models. Lykoudis[22] generalized the Prandtl mixing length concept to MHD for a fully established turbulent channel flow, in a transverse and uniform magnetic field (electrically insulated channel). He obtained an expression for the turbulent stress in the case of MHD based on the solution of an oscillating infinite plate. Damping functions are added to the algebraic model to account for the presence of a magnetic field. The k–ϵ two-equation model has been used in conjunction with MHD flows by several authors. Lee et al.[23] used the k–ϵ model (with no modification) to study the effect of MHD in a three-dimensional channel flow of liquid metal. Frando et al.[24] used the Navier–Stokes equations with the k–ϵ model to determine the steady-state solution of an MHD turbulent flow in an electromagnetic valve. The breaking and accelerating of the flow was demonstrated. El-Kaddah[25] calculated the recirculating flow in an induction furnace using the turbulent Navier–Stokes equations augmented with electromagnetic body forces. Again, the k–ϵ model (with no modification) was used to evaluate the turbulent viscosity. Shimomura[26] derived the exact equations for the turbulent kinetic energy and its dissipation rate based on the two-scale direct interaction approximation approach. The resulting equations, though exact, are very complex and require several closure coefficients, which cannot be clearly determined. However, in some cases, simplifications can be made based on the geometry of the problem.

There are mainly three approaches for the computation of turbulent flows. The direct numerical simulation approach is an exact method in the sense that the original governing equations are solved without any modifications, or filtering process. The second approach is the large-eddy simulation.[27] Large scales are numerically computed, whereas the small scales are modeled by simple eddy viscosity models, known as subgrid scale models. These two methods are very costly in terms of computational time and storage requirement. A more affordable method consists in averaging Navier–Stokes equations in time (called Reynolds averaging). When the filter operation is applied to the equations, the Reynolds averaged Navier–Stokes (RANS) equations are obtained. In this filtering process, additional terms appear, known as the Reynolds stresses. A closure model (or turbulence model) is required to close the system. Tremendous amount of investigation has been conducted in this domain, resulting in many different turbulence models, ranging from simple algebraic models to more sophisticated multi-equation models.[28] Unfortunately, none of the proposed models is able to predict accurately turbulent flows for a wide range of applications. The difficulty in developing such models relies in that the closure constants are based on empiricism and are calibrated to match the experimental data. This makes them nonuniversal and more likely to provide good results only for the type of applications they were designed for. The RANS approach is used for simple engineering

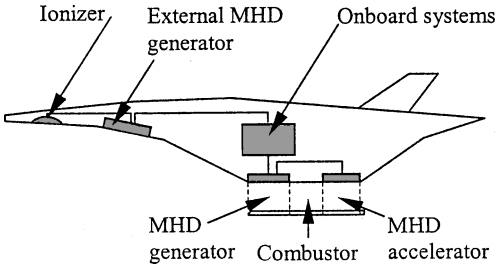

Fig. 1 Simplified schematic of the AJAX concept.

applications because of its relatively low computational cost compared to other existing methods. Because the turbulence models used in RANS are mostly based on empiricism, they have to be tuned for a given application.

The possibility of utilizing MHD flow control for hypersonic vehicles has led to the AJAX concept.[29–32] The AJAX vehicle is a long-range, hypersonic vehicle that employs a coupled MHD generator/accelerator propulsion system. The MHD control is designed to improve the performances of the scramjet. Figure 1 shows a simplified schematic of the MHD system. The external MHD generator controls the inlet of the scramjet. The application of a magnetic field provides a means to control the leading-edge shock wave and adjust the flow rate within the scramjet. Therefore, a fixed-geometry scramjet can be employed. The electricity generated by the MHD generator operates an ionizer, located near the nose of the vehicle. The ionization process increases the electrical conductivity of the plasma, which provides a better MHD interaction. The internal MHD generator slows down the flow before combustion and increases the pressure. The electric power produced is then used to operate onboard systems and the MHD accelerator. The gases exiting the combustion chamber should be of sufficient temperature as not to require additional ionization to reach adequate conductivities.

The investigation of the flowfield over an entire vehicle would require extensive computational resources and is not feasible at the present time. The proposed numerical tools could be used to simulate some major portions of the flowfield over a supersonic vehicle. The flow within the MHD generator and MHD accelerator can be approximated by MHD channel flows. The nose of the vehicle can be represented by a blunt body. Changes in the vehicle geometry can be approximated by compression/expansion corners. The scramjet is a combination of supersonic/hypersonic inlets and channel flows. The remainder of the vehicle can be analyzed by assuming it to be locally a flat plate. In an effort to develop a computational tool able to investigate various MHD flows, the computer program is first compared to available analytical and experimental data of MHD flows over simple geometries. The Reynolds averaged approach is selected to represent turbulence for its low requirement in terms of computational resources. The Baldwin–Lomax turbulence model is modified to account for the presence of a magnetic field.

Governing Equations

Full MHD Equations

The MHD equations are composed of the Maxwell's equations, generalized Ohm's law, continuity, momentum, and energy equations. Maxwell's equations relate the basic electric and magnetic field quantities and how they are produced. The combination of Maxwell's equations, or more specifically, Faraday's law, generalized Ohm's law, and continuity equation results in the magnetic transport equation. The electric field can be eliminated from the equations, leaving only the magnetic field. The resulting MHD equations comprise the continuity, momentum, magnetic transport, and energy equations. The equations are written in a nondimensional conservative form as

$$\frac{\partial \boldsymbol{Q}}{\partial t}+\frac{\partial \boldsymbol{E}}{\partial x}+\frac{\partial \boldsymbol{F}}{\partial y}+\boldsymbol{H}=\frac{\partial \boldsymbol{E}_v}{\partial x}+\frac{\partial \boldsymbol{F}_v}{\partial y} \tag{1}$$

The original system of equations has been shown to be difficult to solve due to singularities in the Jacobian matrices associated with the system because of the existence of zero eigenvalues. One solution that has been proposed[18] is to modify the Jacobian matrices, leading to the introduction of the additional flux vector $\boldsymbol{H}$ in the MHD equations. The unknown vector and flux vectors are given in Eqs. (2a–2d):

$$\boldsymbol{Q}=[\rho \quad \rho u \quad \rho v \quad \rho w \quad B_x \quad B_y \quad B_z \quad \rho e_t]^T \tag{2a}$$

$$\boldsymbol{E}=\begin{bmatrix} \rho u \\ \rho u^2+p+\dfrac{-B_x^2+B_y^2+B_z^2}{2} \\ \rho uv-B_xB_y \\ \rho uw-B_xB_z \\ 0 \\ uB_y-vB_x \\ uB_z-wB_x \\ \cdots\cdots\cdots\cdots\cdots\cdots\cdots \\ \left(\rho e_t+p+\dfrac{B_x^2+B_y^2+B_z^2}{2}\right)u \\ -B_x(uB_x+vB_y+wB_z) \end{bmatrix}$$

$$\boldsymbol{F}=\begin{bmatrix} \rho v \\ \rho vu-B_yB_x \\ \rho v^2+p+\dfrac{B_x^2-B_y^2+B_z^2}{2} \\ \rho vw-B_yB_z \\ vB_x-uB_y \\ 0 \\ vB_z-wB_y \\ \cdots\cdots\cdots\cdots\cdots\cdots\cdots \\ \left(\rho e_t+p+\dfrac{B_x^2+B_y^2+B_z^2}{2}\right)v \\ -B_y(uB_x+vB_y+wB_z) \end{bmatrix} \tag{2b}$$

$$\boldsymbol{H}=\boldsymbol{H}_M\left(\frac{\partial B_x}{\partial x}+\frac{\partial B_y}{\partial y}\right), \qquad \boldsymbol{H}_M=\begin{bmatrix} 0 \\ B_x \\ B_y \\ B_z \\ u \\ v \\ w \\ uB_x+vB_y+wB_z \end{bmatrix} \tag{2c}$$

$$\boldsymbol{E}_v=\begin{bmatrix} 0 \\ \tau_{xx} \\ \tau_{xy} \\ \tau_{xz} \\ \dfrac{1}{Re_{m\infty}\sigma_e}\dfrac{\partial B_x}{\partial x} \\ \dfrac{1}{Re_{m\infty}\sigma_e}\dfrac{\partial B_y}{\partial x} \\ \dfrac{1}{Re_{m\infty}\sigma_e}\dfrac{\partial B_z}{\partial x} \\ u\tau_{xx}+v\tau_{xy}+w\tau_{xz}-q_x \end{bmatrix}$$

$$\boldsymbol{F}_v = \begin{bmatrix} 0 \\ \tau_{yx} \\ \tau_{yy} \\ \tau_{yz} \\ \dfrac{1}{Re_{m\infty}\sigma_e}\dfrac{\partial B_x}{\partial y} \\ \dfrac{1}{Re_{m\infty}\sigma_e}\dfrac{\partial B_y}{\partial y} \\ \dfrac{1}{Re_{m\infty}\sigma_e}\dfrac{\partial B_z}{\partial y} \\ u\tau_{yx} + v\tau_{yy} + w\tau_{yz} - q_y \end{bmatrix} \tag{2d}$$

where

$$\rho e_t = \tfrac{1}{2}\rho(u^2 + v^2 + w^2) + p/(\gamma - 1) + \left(B_x^2 + B_y^2 + B_z^2\right)/2 \tag{3}$$

For a Newtonian fluid,

$$\tau_{ij} = \frac{\mu}{Re_\infty}\left(\frac{\partial u_i}{\partial x_j} + \frac{\partial u_j}{\partial x_i} - \frac{2}{3}\frac{\partial u_k}{\partial x_k}\delta_{ij}\right) \tag{4}$$

and for a perfect gas,

$$q_i = -\frac{\mu}{Re_\infty Pr(\gamma - 1)M_\infty^2}\frac{\partial T}{\partial x_i} \tag{5}$$

The expression of the internal energy in Eq. (3) applies only to nonchemically reacting perfect gases. The nondimensional parameters appearing in the equations are the Reynolds number $Re_\infty = \rho_\infty U_\infty L/\mu_\infty$, the Prandtl number $Pr = \mu_\infty c_p/k$, the magnetic Reynolds number $Re_{m\infty} = \sigma_{e\infty}\mu_{e0}U_\infty L$, and the freestream Mach number M_∞. The magnetic Reynolds number represents the ratio of the magnetic convection to the magnetic diffusion.

The governing MHD equation given by Eq. (1), which is written in the physical space (x, y), is transformed into the computational space (ξ, η) and expressed as

$$\frac{\partial \bar{\boldsymbol{Q}}}{\partial t} + \frac{\partial \bar{\boldsymbol{E}}}{\partial \xi} + \frac{\partial \bar{\boldsymbol{F}}}{\partial \eta} + \bar{\boldsymbol{H}} = \frac{\partial \bar{\boldsymbol{E}}_v}{\partial \xi} + \frac{\partial \bar{\boldsymbol{F}}_v}{\partial \eta} \tag{6}$$

where

$$\bar{\boldsymbol{Q}} = \frac{\boldsymbol{Q}}{J}, \qquad \bar{\boldsymbol{H}} = \boldsymbol{H}_M\left(\frac{\partial \bar{B}_x}{\partial \xi} + \frac{\partial \bar{B}_y}{\partial \eta}\right) \tag{7a}$$

$$\bar{\boldsymbol{E}} = \frac{1}{J}(\xi_x \boldsymbol{E} + \xi_y \boldsymbol{F}), \qquad \bar{\boldsymbol{F}} = \frac{1}{J}(\eta_x \boldsymbol{E} + \eta_y \boldsymbol{F}) \tag{7b}$$

$$\bar{B}_x = \frac{1}{J}(\xi_x B_x + \xi_y B_y), \qquad \bar{B}_y = \frac{1}{J}(\eta_x B_x + \eta_y B_y) \tag{7c}$$

$$\bar{\boldsymbol{E}}_v = \frac{1}{J}(\xi_x \boldsymbol{E}_v + \xi_y \boldsymbol{F}_v), \qquad \bar{\boldsymbol{F}}_v = \frac{1}{J}(\eta_x \boldsymbol{E}_v + \eta_y \boldsymbol{F}_v) \tag{7d}$$

Low Magnetic Reynolds Number Approximation

The numerical simulation of MHD flows typically requires the solution of a system of eight equations: continuity, momentum (three components), energy, and magnetic field induction (three components). For MHD flows that are characterized by a low electrical conductivity, the governing equations can be simplified. The validity of the simplification is monitored by a nondimensional number known as the magnetic Reynolds number. It can be shown that for small values of the magnetic Reynolds number ($Re_{m\infty} \ll 1$) the induced magnetic field is negligible compared to the applied magnetic field. Therefore, when this assumption is valid, the magnetic induction equations do not need to be solved. This is especially appealing because the method applied to solve these equations is source of numerical difficulties. When the full system of MHD equations is solved, it has been experienced to be very difficult for the magnetic field to remain divergence free at all time levels. Numerical techniques have been proposed[18] to alleviate this problem but generally result in more complex equations or additional steps in the numerical procedure. The other source of difficulties is that the MHD equations become stiffer as the magnetic Reynolds number decreases. In the low magnetic Reynolds number approach, the magnetic field automatically satisfies the zero-divergence constraint, provided its initial distribution is divergence free (because it is given and remains constant through the computation). The current density is determined directly from Ohm's law, and the MHD effect is modeled by the introduction of source terms in the Navier–Stokes equations. Under the assumption of small magnetic Reynolds number, the governing equations are

$$\frac{\partial \boldsymbol{Q}}{\partial t} + \frac{\partial \boldsymbol{E}}{\partial x} + \frac{\partial \boldsymbol{F}}{\partial y} = \frac{\partial \boldsymbol{E}_v}{\partial x} + \frac{\partial \boldsymbol{F}_v}{\partial y} + \boldsymbol{S}_{\text{MHD}} \tag{8}$$

The additional source term is represented by $\boldsymbol{S}_{\text{MHD}}$. The unknown and flux vectors are given by Eqs. (9a–9d). The unknown quantities that need to be computed are the density, momentum components, and total energy. The magnetic and electric fields are considered as given quantities and remain constant throughout the computations.

$$\boldsymbol{Q} = [\rho \quad \rho u \quad \rho v \quad \rho w \quad \rho e_t]^T \tag{9a}$$

$$\boldsymbol{E} = \begin{bmatrix} \rho u \\ \rho u^2 + p \\ \rho uv \\ \rho uw \\ (\rho e_t + p)u \end{bmatrix}, \qquad \boldsymbol{F} = \begin{bmatrix} \rho v \\ \rho vu \\ \rho v^2 + p \\ \rho vw \\ (\rho e_t + p)v \end{bmatrix} \tag{9b}$$

$$\boldsymbol{E}_v = \begin{bmatrix} 0 \\ \tau_{xx} \\ \tau_{xy} \\ \tau_{xz} \\ u\tau_{xx} + v\tau_{xy} + w\tau_{xz} - q_x \end{bmatrix}, \qquad \boldsymbol{F}_v = \begin{bmatrix} 0 \\ \tau_{yx} \\ \tau_{yy} \\ \tau_{yz} \\ u\tau_{yx} + v\tau_{yy} + w\tau_{yz} - q_y \end{bmatrix} \tag{9c}$$

$$\boldsymbol{S}_{\mathrm{MHD}} = Re_{m\infty}\begin{bmatrix} 0 \\ B_z(E_y + wB_x - uB_z) - B_y(E_z + uB_y - vB_x) \\ B_x(E_z + uB_y - vB_x) - B_z(E_x + vB_z - wB_y) \\ B_y(E_x + vB_z - wB_y) - B_x(E_y + wB_x - uB_z) \\ E_x(E_x + vB_z - wB_y) + E_y(E_y + wB_x - uB_z) + E_z(E_z + uB_y - vB_x) \end{bmatrix} \tag{9d}$$

where

$$\rho e_t = \tfrac{1}{2}\rho(u^2 + v^2 + w^2) + p/(\gamma - 1) \tag{10}$$

All other quantities have the same definitions as already noted. In contrast with the full MHD equations, the electric field appears explicitly in the formulation associated with the low magnetic Reynolds number approximation. This offers additional control on the flow.[33,34] Equation (8) is transformed into the computational space (ξ, η) as

$$\frac{\partial \bar{\boldsymbol{Q}}}{\partial t} + \frac{\partial \bar{\boldsymbol{E}}}{\partial \xi} + \frac{\partial \bar{\boldsymbol{F}}}{\partial \eta} = \frac{\partial \bar{\boldsymbol{E}}_v}{\partial \xi} + \frac{\partial \bar{\boldsymbol{F}}_v}{\partial \eta} + \bar{\boldsymbol{S}}_{\mathrm{MHD}} \tag{11}$$

where

$$\bar{\boldsymbol{S}}_{\mathrm{MHD}} = (1/J)\boldsymbol{S}_{\mathrm{MHD}} \tag{12}$$

All other flux vectors are obtained similarly to Eqs. (7a) and (7b).

Numerical Scheme

The governing equations are solved by a four-stage Runge–Kutta scheme. It has been selected because of its high order of accuracy (fourth order) and its low storage requirement because only two time levels need to be stored. The spatial derivatives are approximated by second-order central differences.

Some instabilities may arise due to the high order of accuracy associated with the numerical scheme. To alleviate this problem, a postprocess stage is usually required to stabilize the solution. A method that has been successfully employed in the past is the application of a TVD scheme as a postprocess stage. This method has the advantage of automatically adjusting the amount of damping (by switching from second to first order in accuracy) where needed. However, it requires the computation of the eigenvalues and eigenvectors associated with the governing equations. It is also expensive in terms of computational resources. The second-order symmetric TVD scheme with Davis–Yee symmetric limiter has been chosen due to its successful application to MHD problems by previous investigators. It is particularly appealing for high-speed problems involving strong discontinuities such as shock waves. Details of the postprocess stage may be found in Ref. 17.

Baldwin–Lomax Zero-Equation Turbulence Model

The Baldwin–Lomax[35] model is a two-layer model composed of an inner and an outer region. The switch between the inner and outer turbulent viscosity occurs at the y location, where both turbulent viscosities are equal. The basic assumption is that the local rate of production and dissipation of turbulence are approximately equal. This model does not include any convection of turbulence.

In the inner layer, the length scale associated with the turbulence is the mixing length. The mixing length is the distance that lumps of fluid associated with fluctuating quantities travel before they lose their identity. From experimental evidence, it is observed that turbulence damps out near the solid surfaces, within the viscous sublayer. Subsequently, turbulence grows rapidly. In this model, the mixing length is specified by an algebraic function, known as the Van Driest function:

$$l = \kappa y[1 - \exp(-y^+/A^+)] \tag{13}$$

where

$$y^+ = \rho_w u_\tau y/\mu_w \tag{14}$$

$$u_\tau = \sqrt{|\tau_w|/\rho_w} \tag{15}$$

The characteristic velocity is given by $V_t = l\omega$, where

$$\omega = \sqrt{\left(\frac{\partial v}{\partial z} - \frac{\partial w}{\partial y}\right)^2 + \left(\frac{\partial w}{\partial x} - \frac{\partial u}{\partial z}\right)^2 + \left(\frac{\partial u}{\partial y} - \frac{\partial v}{\partial x}\right)^2} \tag{16}$$

Therefore, in the inner layer, the turbulent viscosity is given by

$$\mu_{t_i} = \rho l^2 \omega \tag{17}$$

In the outer region, the turbulent viscosity is given by

$$\mu_{t_o} = \alpha \rho U_0 L_0 \tag{18}$$

where, at a given x,

$$U_0 = \min\{G_{\max}, [(\Delta V)^2/G_{\max}]\} \tag{19}$$

$$G_{\max} = \max[(l/\kappa)\omega] \tag{20}$$

$$L_0 = C_{\mathrm{CP}} I_0 y_{\max} \tag{21}$$

where $y_{\max}$ is the value of y where $G_{\max}$ occurs. $\Delta V = V_{\max} - V_{\min}$ is the difference between the maximum and minimum velocities at a given x. ($V_{\min} = 0$ for boundary-layer flows.) I_0 is the intermittency factor:

$$I_0 = \left[1 + 5.5(C_{\mathrm{kleb}} y/y_{\max})^6\right]^{-1} \tag{22}$$

The closure coefficients for the Baldwin–Lomax model are summarized in Table 1.

Modifications of the Baldwin–Lomax Model for MHD Flows

The generalization of Prandtl mixing length concept was extended to MHD flows at low magnetic Reynolds number by Brouillette and Lykoudis.[22] In the inner region, the turbulent viscosity is now written as

$$\mu_{t_i} = \rho\kappa^2 y^2[1 - \exp(-y^+/A^+)]\gamma_2\gamma_3\omega \tag{23}$$

where

$$\gamma_2 = 1 - \exp\left\{-(y^+/A^+)\left[\sqrt{\tfrac{1}{2}(A^+\lambda)^4 + 1} + \tfrac{1}{2}(A^+\lambda)^2\right]^{\frac{1}{2}}\right\} \tag{24}$$

Table 1 Closure coefficients for the Baldwin–Lomax model

Coefficient	Value
κ	0.41
C_{CP}	1.6
C_{Kleb}	0.3
A^+	26.0
α	0.0168

$$\gamma_3 = \exp(-A\lambda^2), \qquad A = 700 \tag{25}$$

$$\lambda^2 = \sigma_e B^2 \mu \Big/ \rho \tau_w \tag{26}$$

The damping functions γ_1 and γ_2, as well as their associated constants, have been designed to match their experimental investigation of a channel flow of an electrically conducting fluid subject to a uniform transverse magnetic field.[36] It has been observed that when the skin friction is plotted vs the Hartmann number (while keeping the Reynolds number constant), all curves coincide on the same laminar line when the ratio Ha/Re is larger than 1/225. This illustrates that the presence of a magnetic field tends to inhibit turbulence or initiates a relaminarization process. The main idea behind the damping functions introduced by Brouillette and Lykoudis[22] is that the magnetic field leads to a suppression of the correlation term $\overline{u'v'}$. The damping functions were designed for flows with a transverse magnetic field, such that the damping acts directly on the u' fluctuation. (The v' fluctuation is parallel to the transverse magnetic field.)

Results

MHD Rayleigh Problem

The MHD Rayleigh problem is a key benchmark problem for MHD flows. It is a time-accurate problem that involves molecular viscosity, magnetic diffusivity, and wave propagation. This test case is used to validate the ability of the numerical code to compute accurately boundary-layer type of flows. Consider an infinite flat plate at rest in a motionless electrically conducting fluid. A constant magnetic field B_0 is applied in the y direction, that is, perpendicular to the plate. At time $t = 0.0$, the plate is suddenly set into motion in the x direction, that is, in the direction of the plate, at a constant speed of U_0. Figure 2 shows a typical velocity profile obtained for the MHD Rayleigh flow. The motion of the plate drives the fluid near the plate, and the motion propagates within the fluid as time increases. The wave front separates the region where the fluid is at rest (ahead of the wave front) and the region where the fluid is accelerating (near the wall). The latter is referred to as the Hartmann layer and has a thickness of $\delta_H = \sqrt{(\rho\nu/\sigma_e)}/B_0$. The velocity field induces a magnetic field that propagates in the y direction as a plane wave, which is called the Alfvèn wave. It travels at the constant speed $A_0 = B_0/\sqrt{(\mu_{e0}\rho)}$ (Alfvèn speed). For the case where the magnetic Prandtl number, that is, the ratio of kinematic viscosity to magnetic diffusivity, equals unity, there exists an analytical solution (see Ref. 37) in terms of velocity and induced magnetic fields. The MHD Rayleigh flow has been computed and compared with the analytical solution for the case given in Table 2.

Table 2 Summary of the MHD Rayleigh problem parameters

Property	Value
Electrical conductivity	$\sigma_e = 10^7/4\pi$ mho/m
Fluid density	$\rho = 0.4 \times 10^{-4}$ kg/m^3
Applied magnetic field	$B_0 = 1.449 \times 10^{-4}$ T
Vertical range of the domain	$0 \le y \le 2.5$ m
Time interval	$0 \le t \le 0.06$ s

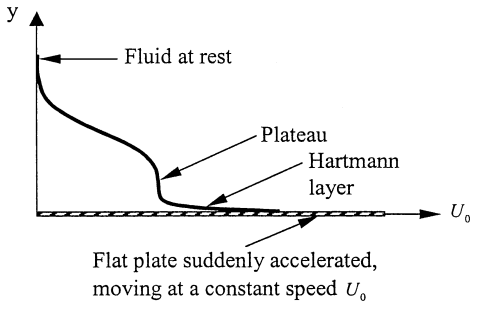

Fig. 2 Schematic of the MHD Rayleigh flow.

Table 3 Flow properties of the supersonic flow over a blunt body

Flow property	Value
Mach number	$M_\infty = 2.97$
Freestream velocity	$u_\infty = 3625$ m/s
Freestream density	$\rho_\infty = 3.035 \times 10^{-5}$ kg/m^3
Freestream pressure	$p_\infty = 32.3$ Pa
Freestream temperature	$T_\infty = 3708$ K

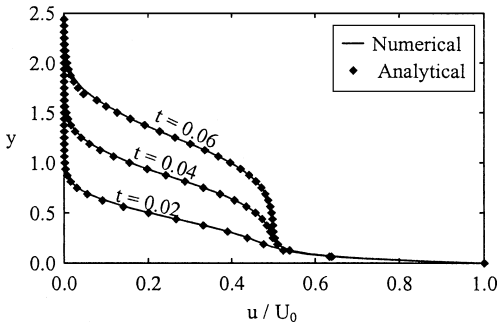

Fig. 3 Velocity profiles for the MHD Rayleigh problem (electrically insulating wall).

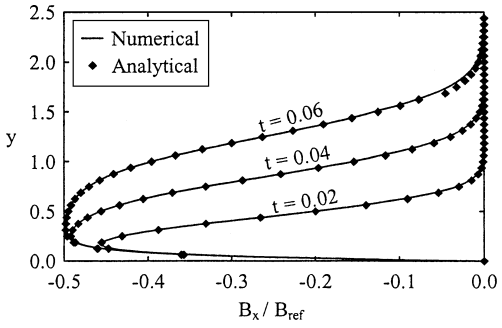

Fig. 4 Induced magnetic field profiles for the MHD Rayleigh problem (electrically insulating wall).

The magnetic Reynolds number based on the height of the domain is $Re_m = 2.5$, and, therefore, the full MHD equations are solved. The temperature of the flow has been adjusted such that the kinematic viscosity, calculated from Sutherland's law, equals the magnetic diffusivity. Two types of boundary conditions are investigated for the flat plate. For an electrically insulated wall, the magnetic field is specified at the wall. For a perfectly conducting wall, the magnetic field is extrapolated at the wall (zero normal gradient). Figures 3 and 4 show the velocity profiles and induced magnetic fields obtained for $t \le 0.06$ s in the case of an electrically insulating wall. The numerical solutions show good agreement with the analytical solutions. All of the features of Fig. 2 are represented. Figures 5 and 6 show the velocity profiles and induced magnetic fields for the case of a perfectly conducting wall. In this case, the Hartmann layer is not present. Good agreement between the analytical and numerical solutions is obtained.

Supersonic MHD Flow over a Blunt Body

In this section, the supersonic flow over a blunt body is computed and the shock standoff distance is compared to the analytical solution proposed by Lykoudis.[5] The inflow conditions are given in Table 3.

The blunt-body radius of curvature is $r_b = 0.025$ m. The grid system is shown in Fig. 7. The magnetic field is initially oriented in the y direction, and the conductivity is assumed to be constant ($\sigma_e = 800$ mho/m) for all of the computations. All flow properties are specified at the far field, including the magnetic field. The blunt

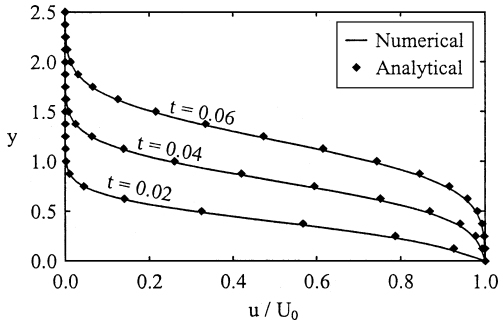

Fig. 5 Velocity profiles for the MHD Rayleigh problem (perfectly conducting wall).

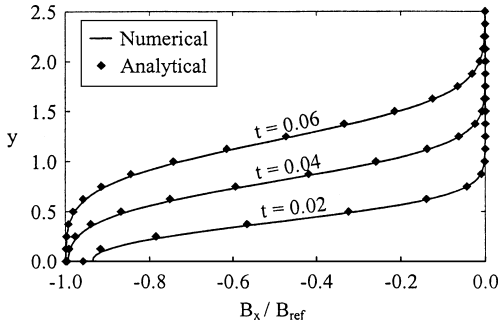

Fig. 6 Induced magnetic field profiles for the MHD Rayleigh problem (perfectly conducting wall).

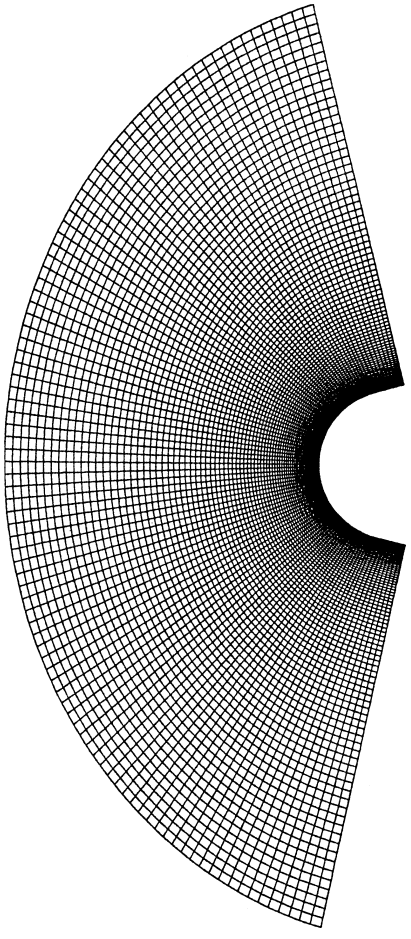

Fig. 7 Grid configuration for the blunt body (100 × 80 grid points).

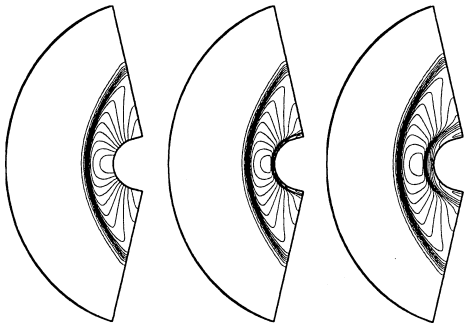

a) $B_y = 0.0$ T b) $B_y = 0.025$ T c) $B_y = 0.035$ T

Fig. 8 Pressure contours for various magnetic field intensities.

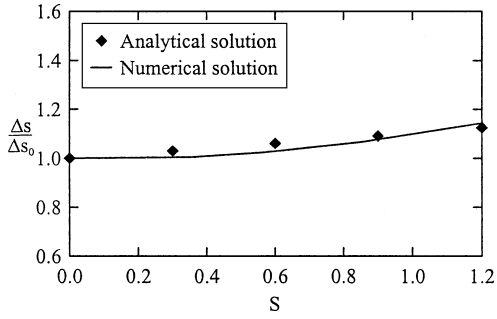

Fig. 9 Shock standoff distance for the supersonic flow over a blunt body.

body is considered to act as an adiabatic wall, and the magnetic field is imposed along the wall.

The shock standoff distance moves away from the body as the magnetic field is increased (Fig. 8). When the magnetic field is oriented in the y direction, the body force created by the magnetic field is acting in the opposite direction of the incoming velocity, which slows down the flow. Because the velocity is decreased in the region between the blunt body and the shock wave, a wider area is required for the fluid passage, and therefore, the shock standoff distance has to increase. In the analytical solution proposed by Lykoudis,[5] the shock standoff distance ratio between the MHD and no-magnetic case is a function of the density ratio across the shock and the interaction parameter $S = \sigma_e B^2 r / \rho_\infty u_\infty$. The numerical results are compared with the analytical solution in Fig. 9. Δs and Δs_0 are the nondimensional shock standoff distances with and without a magnetic field, respectively. The standoff distances have been nondimensionalized by the radius of curvature of the shock. Small discrepancies between the analytical solution and numerical results can be explained by the difficulty to reproduce the assumptions made to derive the analytical solution. For example, it is assumed that the magnetic field remains constant in the region between the shock and the body and is perpendicular to the incoming streamlines. In the numerical simulation, an induced magnetic field is generated, which is combined with the applied magnetic field. Lykoudis also assumed that the pressure was not altered by the magnetic field in the stagnation region. (A Newtonian pressure distribution with constant density is assumed.) This assumption cannot be reproduced numerically because the stagnation pressure is decreased when the magnetic field intensity increases.

Hartmann Flow

The fully developed flow between two parallel plates under a transverse magnetic field is investigated under the influence of a magnetic field. It is the equivalent to the Couette flow in fluid mechanics. The term fully developed refers to the velocity profile being independent of the axial coordinate. A pressure gradient exists in the longitudinal coordinate, which drives the fluid into motion and balances the viscous and magnetic friction. This type of flow is the

simplest MHD channel flow and was first investigated by Hartmann in 1930. The presence of a magnetic field alone can only slow the flow, and a larger pressure gradient is required to maintain the same mass flow rate. The Hartmann flow has been extended to the case where both a magnetic and electric fields are present. In this case, it is possible to decelerate or accelerate the flow by a suitable combination of the electric and magnetic fields. Here, both laminar and turbulent flows are considered and compared with analytical or experimental results. This test case serves as a basis for the calibration of the modified turbulence models.

Consider an incompressible fluid, with constant viscosity and constant electrical conductivity flowing between two infinite parallel flat plates (Fig. 10). A constant magnetic field is applied in the transverse direction, that is, the y direction. There is no applied electric field. All variables are functions of y only, except the pressure. The walls are located at $y = \pm h$. Laminar and turbulent flows are investigated under the conditions given in Table 4.

The Reynolds number, based on the half-height h between the two plates and the average velocity, ranges from 5×10^3 to 5×10^4. The magnetic Reynolds number corresponding to these conditions is $Re_m = 1.51 \times 10^{-4}$. Therefore, the induced magnetic field can be considered negligible compared to the applied magnetic field. In fact, the value of the induced magnetic field can be analytically evaluated in the general case.[37] Figure 11 shows the magnitude of the induced magnetic field b_x compared to the applied field B_0 (theoretical distribution). It can be observed that for a given Hartmann number, the induced field is maximum at the wall and zero at the centerline. The ratio b_x/B_0 decreases as the Hartmann number increases. In all cases, the induced magnetic field is negligible compared to the applied field. In fact, the largest value of the induced field is more than 2000 times smaller than the applied field. Therefore, the low magnetic Reynolds number approximation can be considered valid for this application.

Table 4 Properties of the MHD Hartmann flow

Property	Value
Density	$\rho = 1.225$ kg/m^3
Electrical conductivity	$\sigma_e = 800$ mho/m
Viscosity	$\mu = 1.8 \times 10^{-5}$ kg/(m · s)
Distance between the plates	$h = 0.005$ m

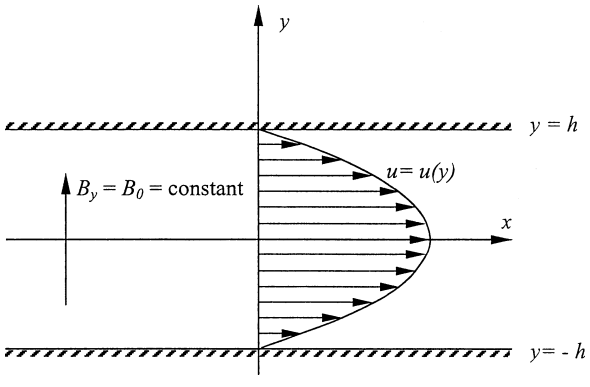

Fig. 10 Schematic of the Hartmann flow.

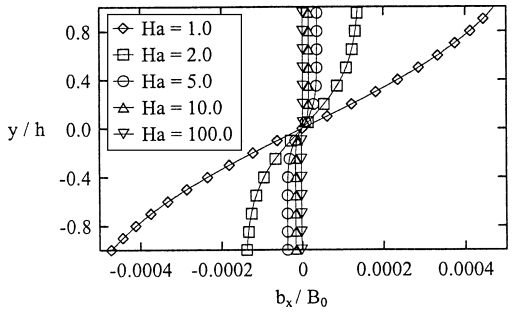

Fig. 11 Analytical distribution of the induced magnetic field.

The computation is performed on a two-dimensional domain. To obtain a fully developed flow, the length of the numerical domain should be much larger than its height. This requires a large number of grid points in the x direction and results in a prohibitive computational time for such a simple case. However, it is possible to accelerate the convergence of the code, by having a small computational domain and modifying the boundary conditions. The ratio between the length and the height of the domain is $L/2h = 10$, and the number of grid points in the x direction is 10, with uniform grid spacing. There are 150 grid points in the y direction, and grid clustering is implemented near the two solid walls to resolve the velocity gradients. The velocity is extrapolated at the inlet and outlet to obtain a fully developed flow in a short computational time. The pressure gradient in the x direction is adjusted to provide the same mass flow rate regardless of the strength of the magnetic field. The convergence criterion is based on the change in pressure between two successive iterations, calculated over the entire domain of solution. Convergence is achieved when the change in pressure has decreased by four orders of magnitude.

Laminar Flow

In the case of a laminar flow, an analytical solution exists.[38] It can be simplified further because the magnetic Reynolds number is small. The pressure gradient balances the Lorentz force induced by the interaction between the magnetic field and velocity field. The magnetic field that is applied in the positive y direction with a magnitude of B_0. The Hartmann number, defined as $Ha = B_0 h \sqrt{(\sigma_e/\mu)}$, is a nondimensional parameter, the square of which represents a measure of the ratio of the electromagnetic to viscous forces. Note that the reference length associated with the Hartmann number should represent a characteristic length of the variation of u.

In the case of a turbulent flow, it has been experimentally shown by Brouillette and Lykoudis[36] that a relaminarization process should occur when the magnetic field is sufficiently strong. The criterion for the relaminarization process is expressed by the ratio of the Hartmann number to the Reynolds number. The advantage of expressing the relaminarization criterion by this ratio is that it becomes independent of the reference length. Brouillette and Lykoudis found that when the critical value of $Ha/Re = 1/225$ is reached, the flow should return to a laminar state. The goal of this investigation is to verify this experimental conclusion.

Figure 12 shows the fully developed velocity profile for different values of the Hartmann number in the laminar case, for which a comparison with the analytical solution is possible. The velocities are normalized with the maximum velocity obtained in the nonmagnetic laminar case. When $Ha = 0.0$, the well-known parabolic profile corresponding to the Couette flow in fluid dynamic is obtained. As the Hartmann number is increased, the velocity profiles are flattened, the maximum velocity (at the centerline) decreasing.

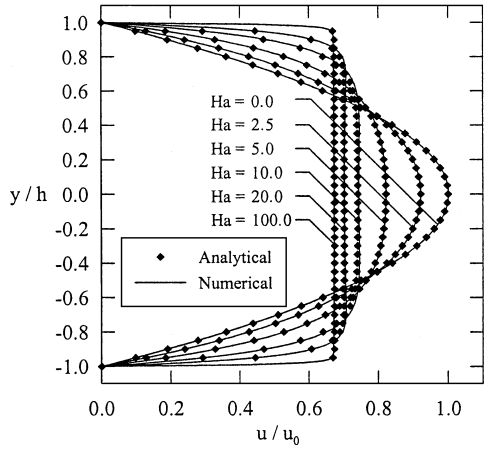

Fig. 12 Laminar velocity profiles for the Hartmann flow.

For Hartmann numbers greater than 10.0, the velocity remains almost constant on a large portion between the two flat plates. It can be qualitatively observed by inspecting the velocity slopes at the walls that the skin friction increases with the Hartmann number. In all cases, the computed solutions are in excellent agreement with the analytical results.

Turbulent Flow

The skin-friction coefficient is plotted vs the ratio Ha/Re in Fig. 13 for a Reynolds number of 1×10^4. In the case of the laminar flow, the computed values compare well with the analytical solution. Note that for large values of the Hartmann number, the skin-friction coefficient can be approximated by the straight line $2Ha/Re$. In the case of the turbulent flow, the skin friction obtained with the original model does not show any relaminarization process, the turbulent skin friction always remains greater than the laminar one. When the damping terms are implemented to provide the modified Baldwin–Lomax model, the relaminarization process takes place at the anticipated location ($Ha/Re \approx 1/225$). As expected, both original and modified models provide the same skin friction in the nonmagnetic case. The turbulent velocity profiles are shown in Fig. 14a for the original model and Fig. 14b for the modified model. The velocities are normalized with the maximum velocity obtained in the nonmagnetic turbulent case. When $Ha = 0.0$, the velocity profile is flatter than in the laminar case, as expected. However, the effect of the magnetic field is less important for small values of Ha than it was for the laminar case. In fact, the velocity profiles remain almost identical until the Hartmann number approaches a value of 10.0 (not shown). For values of Hartmann number Ha greater than 10.0, the velocity flattening becomes noticeable. For large values of the Hartmann number, the shape of the velocity profile is identical to the laminar profile, suggesting that a relaminarization process has occurred. No significant difference in velocity profiles is noticeable between the two versions of the Baldwin–Lomax model.

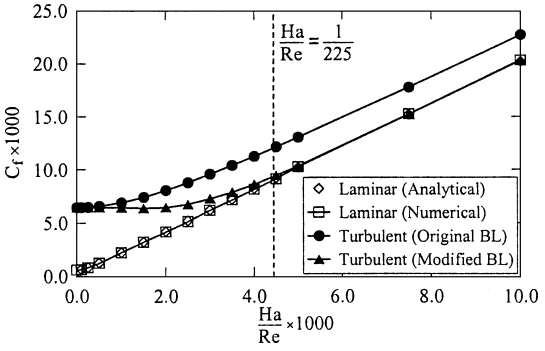

Fig. 13 Skin-friction coefficient for the Hartmann flow at $Re = 1.0 \times 10^4$.

Figure 15a shows the distributions of the turbulent viscosity obtained with the original model. At low Hartmann numbers, the profiles exhibit sharp corners, with a relative minimum at the centerline. As the Hartmann number increases, the amount of turbulent viscosity decreases, and the profiles become more round in shape. The sharp profiles are most likely due to the algebraic nature of the turbulence model and the definition of the mixing length on which the model is based. The modified model provides similar turbulent viscosity profiles (Fig. 15b). For low Hartmann numbers, the turbulent viscosity begins to increase slightly, followed by a rapid decrease, which is faster than when the original model was employed. For example, there is almost no turbulent viscosity produced by the modified model when $Ha = 30.0$, whereas the original model provided more turbulent viscosity. When the maximum turbulent viscosity is plotted vs Ha/Re (Fig. 16), it can be seen that, at the relaminarization point, the original model still provides a substantial amount of turbulent viscosity, whereas the damping terms in the modified version bring the turbulent viscosity to such a low level that the flow can be considered laminar.

Similar results are obtained in terms of skin-friction coefficient, at different Reynolds numbers, ranging from 5×10^3 to 5×10^4 (Fig. 17). In all cases, the original model does not yield any relaminarization process, whereas the modified version shows that the flow becomes laminar at about the same ratio of $Ha/Re \approx 1/225$.

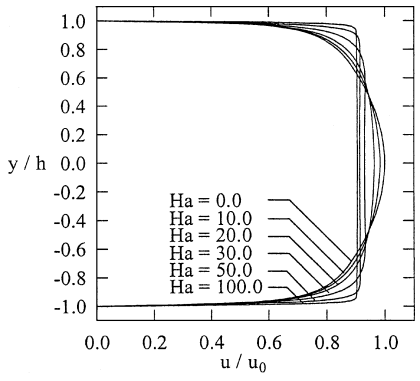

a) Original Baldwin–Lomax model

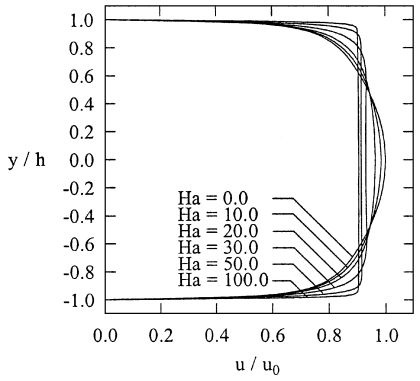

b) Modified Baldwin–Lomax model

Fig. 14 Turbulent velocity profiles.

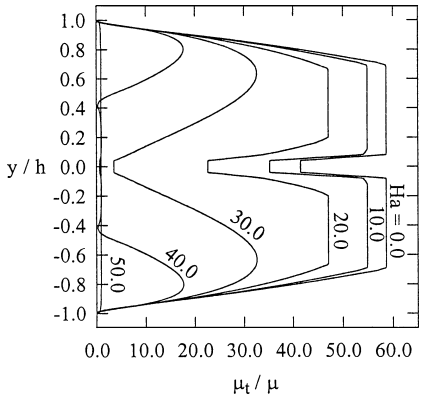

a) Original Baldwin–Lomax model

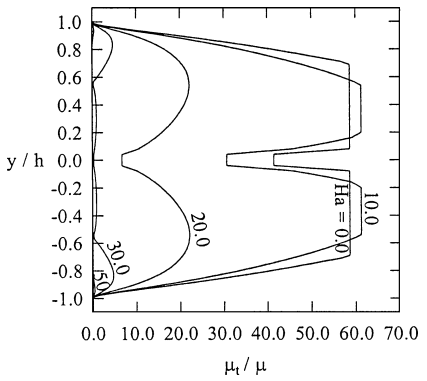

b) Modified Baldwin–Lomax model

Fig. 15 Turbulent viscosity profiles.

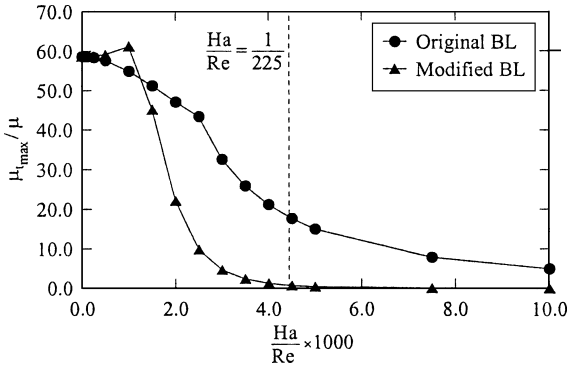

Fig. 16 Maximum turbulent viscosity.

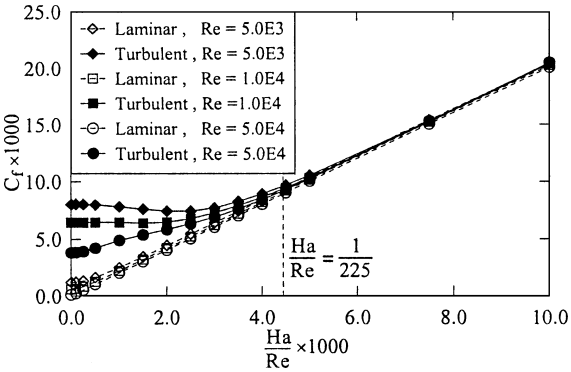

Fig. 17 Effect of the Reynolds number on the skin-friction coefficient.

Conclusions

The computations of laminar and turbulent MHD flows were presented. Two formulations for the MHD equations were considered. The full MHD equations were solved for high-conductivity fluids, whereas the low magnetic Reynolds number formulation was employed for flows characterized by low electrical conductivity. The latter formulation did not require the solution of the magnetic induction equation because the induced magnetic field is negligible compared to the applied magnetic field. The equations of motions were solved by a fourth-order, four-stage Runge–Kutta scheme augmented with a TVD scheme. The equations were written in a flux vector form and nondimensionalized before the application of the numerical scheme. The MHD solver was validated for the MHD Rayleigh flow. Good agreement was found with the existing analytical solution. The location of the shock wave was accurately predicted for the supersonic flow over a blunt body. The Baldwin–Lomax zero-equation turbulence model was implemented to represent turbulence. It was modified to account for the presence of a magnetic field in the case of the turbulent Hartmann flow. The objective was to confirm the experimental observation of a relaminarization process occurring when the Ha/Re ratio becomes larger than 1/225. When the Baldwin–Lomax model was used in its original form, it overpredicted the skin friction and no relaminarization occurred. The modification resulted in the accurate prediction of the relaminarization process, which was not affected by Reynolds numbers in the range of 5×10^3–5×10^4.

Acknowledgments

This work was sponsored by the U.S. Air Force Office of Scientific Research, under tasks monitored by John Schmisseur. The authors acknowledge the support of Kansas National Science Foundation Cooperative Agreement EPS-9874732 and the Wichita State University High Performance Computing Center.

References

[1]Rossow, V. J., "On Flow of Electrically Conducting Fluids over a Flat Plate in the Presence of a Transverse Magnetic Field," NACA TN 3971, May 1957.

[2]Lykoudis, P. S., "On a Class of Compressible Laminar Boundary Layers with Pressure Gradient for an Electrically Conducting Fluid in the Presence of a Magnetic Field," *Proceedings of the 9th Annual Congress of the International Astronautical Federation*, Springer-Verlag, Vienna, 1959, pp. 168–180.

[3]Bleviss, Z. O., "Magnetogasdynamics of Hypersonic Couette Flow," *Journal of the Aero/Space Sciences*, Vol. 25, No. 10, 1958, pp. 601–615.

[4]Bush, W. B., "Magnetohydrodynamic-Hypersonic Flow past a Blunt Body," *Journal of the Aero/Space Sciences*, Vol. 25, No. 11, 1958, pp. 685–690.

[5]Lykoudis, P. S., "The Newtonian Approximation in Magnetic Hypersonic Stagnation-Point Flow," *Journal of the Aero/Space Science*, Vol. 28, No. 7, 1961, pp. 541–546.

[6]Palmer, G., "Magnetic Field Effects on the Computed Flow over a Mars Return Aerobrake," *Journal of Thermophysics and Heat Transfer*, Vol. 7, No. 2, 1993, pp. 294–301.

[7]Zachary, A. L., and Collella, P., "A Higher-Order Godunov Method for the Equations of Ideal Magnetohydrodynamics," *Journal of Computational Physics*, Vol. 99, No. 2, 1992, pp. 341–347.

[8]Bell, J. B., Colella, P., and Trangenstein, J. A., "High Order Godunov Methods for General Systems of Hyperbolic Conservation Laws," *Journal of Computational Physics*, Vol. 82, No. 2, 1989, pp. 362–397.

[9]Brio, M., and Wu, C. C., "An Upwind Differencing Scheme for the Equations of Ideal Magnetohydrodynamics," *Journal of Computational Physics*, Vol. 75, No. 2, 1998, pp. 400–422.

[10]Dai, W., and Woodward, P. R., "Extension of the Piecewise Parabolic Method to Multidimensional Ideal Magnetohydrodynamics," *Journal of Computational Physics*, Vol. 115, No. 2, 1994, pp. 485–514.

[11]Dai, W., and Woodward, P. R., "A Simple Riemann Solver and High-Order Godunov Schemes for Hyperbolic Systems of Conservation Laws," *Journal of Computational Physics*, Vol. 121, No. 1, 1995, pp. 51–65.

[12]Dai, W., and Woodward, P. R., "A Second-Order Iterative Implicit-Explicit Hybrid Scheme for Hyperbolic Systems of Conservation Laws," *Journal of Computational Physics*, Vol. 128, No. 1, 1996, pp. 181–196.

[13]Harada, S., Augustinus, J., Hoffmann, K. A., and Agarwal, R. K., "Development of a Modified Runge–Kutta Scheme with TVD Limiters for the Ideal 1-D MHD Equations," AIAA Paper 97-2090, June 1997.

[14]Augustinus, J., Harada, S., Hoffmann, K. A., and Agarwal, R. K., "Numerical Solution of the Eight-Wave Structure Ideal MHD Equations by Modified Runge–Kutta Scheme with TVD," AIAA Paper 97-2398, June 1997.

[15]Augustinus, J., Hoffmann, K. A., and Harada, S., "Effect of Magnetic Field on the Structure of High-Speed Flows," *Journal of Spacecraft and Rockets*, Vol. 35, No. 5, 1998, pp. 639–646.

[16]Harada, S., Hoffmann, K. A., and Augustinus, J., "Numerical Solution of the Ideal Magnetohydrodynamics Equations for a Supersonic Channel Flow," *Journal of Thermophysics and Heat Transfer*, Vol. 12, No. 4, 1998, pp. 507–513.

[17]Harada, S., Hoffmann, K. A., and Augustinus, J., "Development of a Modified Runge–Kutta Scheme with TVD Limiters for the Ideal Two-Dimensional MHD Equations," AIAA Paper 98-0981, Jan. 1998.

[18]Powell, K. G., Roe, P. L., Myong, R. S., Gombosi, T., and De Zeeuw, D., "An Upwind Scheme for Magnetohydrodynamics," AIAA Paper 95-1704, June 1995.

[19]Hoffmann, K. A., Damevin, H. M., Dietiker, J. F., "Numerical Simulation of Hypersonic Magnetohydrodynamic Flows," AIAA Paper 2000-2259, June 2000.

[20]Ferraro, V. C. A., and Plumton, C., *Magneto-Fluid Mechanics*, 2nd ed., Oxford Univ. Press, Oxford, 1966.

[21]Lykoudis, P. S., "Transition from Laminar to Turbulent Flow in Magneto-Fluid Mechanic Channels," *Review of Modern Physics*, Vol. 32, No. 4, 1960, pp. 796–798.

[22]Brouillette, E. C., and Lykoudis, P. S., "Magneto Fluid Mechanics Channel Flow. II," *Physics of Fluids*, Vol. 10, No. 5, 1967, pp. 1002–1007.

[23]Lee, M. L., Lee, S. J., and Kim, C. T., "Numerical and Experimental Investigation of Flow Channel," *Progress in Fluid Flow Research: Turbulence and Applied MHD*, edited by H. Branover and Y. Unger, Vol. 182, Progress in Astronautics and Aeronautics, AIAA, Reston, VA, 1998, pp. 437–453.

[24]Frando, S., Pesteanu, O., and Fireteanu, V., "Study of the MHD Turbulent Flow in Electromagnetic Valve," *Progress in Fluid Flow Research: Turbulence and Applied MHD*, edited by H. Branover and Y. Unger, Vol. 182, Progress in Astronautics and Aeronautics, AIAA, Reston, VA, 1998, pp. 563–576.

[25]El-Kaddah, N.,"The Turbulent Recirculating Flow Field in a Coreless Induction Furnace, A Comparison of Theoretical Predictions with Measurements," *Journal of Fluid Mechanics*, Vol. 133, No. 37, 1983, pp. 37–46.

[26]Shimomura, Y., "Statistical Analysis of Magnetohydrodynamic Turbulent Shear Flows at Low Magnetic Reynolds Number," *Journal of the Physical Society of Japan*, Vol. 57, No. 7, 1988, pp. 2365–2385.

[27]Lesieur, M., and Comte, P., "Large Eddy Simulations of Compressible Turbulent Flows," *Turbulence in Compressible Flows*, AGARD, Rept. 819, 1997, Chap. 4.

[28]Hoffmann, K. A., and Chiang, S. T., *Computational Fluid Dynamics*, Vol. 3, 4th ed., Engineering Education System, Wichita, KS, 2001.

[29]Bruno, C., and Czysz, P. A., "Electro-Magnetic-Chemical Hypersonic Propulsion System," AIAA Paper 98-1582, April 1998.

[30]Bruno, C., Czysz, P. A., and Murthy, S. N. B., "Electro-Magnetic Interactions in Hypersonic Propulsion Systems," AIAA Paper 97-3389, July 1997.

[31]Burakhanov, B., Likhachev, A., Medin, S., Novikov, V., Okunev, V., and Rickman, V., "Advancement of Scramjet MHD Concept," AIAA Paper 2000-0614, Jan. 2000.

[32]Chase, R. L., Boyd, R., Czysz, P., Froning, H. D., Jr, Lewis, M., and McKinney, L. E., "An Ajax Technology Advanced SSTO Design Concept," AIAA Paper 98-5527, Sept. 1998.

[33]Crawford, C. H., and Karniadakis, G. E. M., "Reynolds Stress Analysis of EMHD-Controlled Wall Turbulence. Part I. Streamwise Forcing," *Physics of Fluids*, Vol. 9, No. 3, 1997, pp. 788–806.

[34]Gaitonde, D. V., and Poggie, J., "Simulation of MHD Flow Control Techniques," AIAA Paper 2000-2326, June 2000.

[35]Baldwin, B. S., and Lomax, H., "Thin Layer Approximation and Algebraic Model for Separated Turbulent Flows," AIAA Paper 78-257, Jan. 1978.

[36]Brouillette, E. C., and Lykoudis, P. S., "Magneto Fluid Mechanics Channel Flow. I Experiment," *Physics of Fluids*, Vol. 10, No. 5, 1967, pp. 995–1001.

[37]Moreau, R., *Magnetohydrodynamics*, Kluwer Academic, Dordrecht, The Netherlands, 1990, pp. 165–171.

[38]Hughes, W. F., and Young, F. J., *The Electromagnetodynamics of Fluids*, 1st ed., Wiley, New York, 1966, Chap. 7.

A. D. Ketsdever
Associate Editor